

Efficient Quantification of Soluble and Insoluble Oxalates in Clay Mineral Mixtures

Teneille Nel^a, Catherine E. Clarke^a, Michele L. Francis^a, Wendy Stone^b, Don A. Cowan^c, Alfred Botha^d, and Timothy Gallagher^e

^aDepartment of Soil Science, Stellenbosch University, Stellenbosch, South Africa; ^bDepartment of Microbiology, Stellenbosch University, Stellenbosch University Water Institute, Stellenbosch, South Africa; ^cCentre for Microbial Ecology and Genomics, Department of Biochemistry, Genetics and Microbiology, University of Pretoria, Genomics Research Institute, Pretoria, South Africa; ^dDepartment of Microbiology, Stellenbosch University, Stellenbosch, South Africa; ^eDepartment of Earth Sciences, Kent State University, Kent, Ohio, USA

ABSTRACT

Quantification of oxalate salts in soil clay minerals is necessary to study oxalate biogeochemistry, but existing analytical techniques are expensive and time-consuming. We aim to develop an efficient attenuated total reflectance mid-infrared (MIR) spectroscopic technique to quantify oxalate salts in a clay mineral matrix. We calibrated MIR models for analysis of oxalate anion concentrations in standard solutions (0–0.01 M) by using a partial least-squares regression algorithm. MIR models were also developed for analysis of sodium oxalate (NaOx) and calcium oxalate (CaOx) content in clay mineral mixtures with composition like soils of a semi-arid region and with contrasting concentrations (0–1.0 g g⁻¹ for both oxalate salts) to test sensitivity of analyses. Validation plots (true vs predicted values) showed excellent model fit ($R^2 \geq 0.96$) and accuracy (normalized root mean squared error of prediction ≤ 0.06) for CaOx, NaOx and oxalic acid components. Once predictive models are stored in analytical software, MIR spectroscopic analyses of samples are much more efficient than chemical techniques. Our MIR spectral-based models are suitable for direct quantification of oxalate salts in clay mineral mixtures for samples like those used for model calibration.

ARTICLE HISTORY



Received 14 December 2022
Accepted 26 March 2024

KEYWORDS

Insoluble oxalates;
nondestructive analysis;
soluble oxalates; whewellite

Introduction

Oxalate salts are the most abundant ionic biominerals on Earth (Cheng et al. 2016; Dauer and Perakis 2013). The stability of the calcium oxalate mineral on geological timescales as well as their biological origin make these minerals a useful tracer of geochemical transformations of organic matter (Cheng et al. 2016; Hofmann and Bernasconi 1998). We use the term Ca oxalate or ‘CaOx’ in the same sense as Uren (Uren 2018), which includes forms in both hydration states, whewellite (CaC₂O₄·H₂O) and weddellite (CaC₂O₄·2H₂O). Calcium oxalates are synthesized by nearly all plants (Franceschi and Horner 1980a) and fulfill various structural and biological functions (Arnott and Webb 2013; Modenesi et al. 2000; Nakata 2003; Pyro et al. 2013; Ross et al. 1999; Tooulakou et al. 2016). CaOx may influence short- and long-term carbon (C) and nutrient supply in ecosystems due to deposition of leaf litter in soils (Dauer and Perakis 2014) and oxalic acid exudation by plant roots (Graustein, Kermit, and Sollins 2011; Jilling et al. 2021; Johnston and Vestal 1993; Pantigoso et al. 2021; Vives-Peris et al. 2020). The role of CaOx in ecosystem calcium (Ca) and C cycling is receiving more attention due to a growing awareness

CONTACT Catherine E. Clarke  cdowding@sun.ac.za  Department of Soil Science, Stellenbosch University, Stellenbosch 7602, South Africa

© 2024 The Author(s). Published with license by Taylor & Francis Group, LLC.

This is an Open Access article distributed under the terms of the Creative Commons Attribution-NonCommercial-NoDerivatives License (<http://creativecommons.org/licenses/by-nc-nd/4.0/>), which permits non-commercial re-use, distribution, and reproduction in any medium, provided the original work is properly cited, and is not altered, transformed, or built upon in any way. The terms on which this article has been published allow the posting of the Accepted Manuscript in a repository by the author(s) or with their consent.

of the importance of biomineralization as a soil carbon sequestration mechanism (Bailey, Buso, and Likens 2003; Braissant et al. 2004; Cailleau, Braissant, and Verrecchia 2011a, 2014; Dauer and Perakis 2014; Hervé et al. 2021; Krieger et al. 2017; Martin et al. 2012; Rehman et al. 2021; Uren 2018). Calcium carbonate (CaCO_3) formation is favored by degradation of CaOx by oxalotrophic bacteria accompanied by an increase in soil pH in a process known as the oxalate-carbonate pathway (OCP) (Braissant, Verrecchia, and Aragno 2002; Cailleau et al. 2014; Uren 2018; Verrecchia, Braissant, and Cailleau 2006) which may be an important mode of atmospheric carbon sequestration (Cailleau, Braissant, and Verrecchia 2011b; Francis and Poch 2019; Hervé et al. 2021; Pons et al. 2018; Rowley et al. 2017; Uren 2018).

The fate of CaOx in soil depends on factors such as soil pH, clay sorption properties, interactions with redox reactive compounds and microbial activity (Dutton and Evans 1996). However, turnover rates of CaOx in soils remain largely unknown (Dauer and Perakis 2013, 2014), as accurate quantification of CaOx has proven to be a significant obstacle. Oxalates in plants occur mainly in the form of insoluble CaOx crystals ($K_{sp} 2.57 \times 10^{-9}$) as well as soluble oxalic acid and sodium or potassium oxalate salts (with sodium oxalate or 'NaOx' being the most common water-soluble form in plants) (Franceschi and Horner 1980b; Ilarslan et al. 1997; Liu et al. 2015). Distinction between insoluble and soluble oxalates is thus crucial for oxalate quantification procedures in studies of OCP function, which operates via transformation of insoluble CaOx. A high-throughput, cost-effective method for measuring oxalate salts in geological materials would advance our understanding of the importance of CaOx in environmental carbon and nutrient cycles.

Current techniques to quantify oxalates include Raman spectroscopy and analysis of sample extracts by colorimetric assays, ion chromatography (IC), high-performance liquid chromatography (HPLC), liquid chromatography tandem mass spectrometry (LC-MS), enzymatic methods and electrochemical techniques (Kotani et al. 2023; Misiewicz et al. 2023; Varão Moura et al. 2022; Vasant Naik Bharati Vidyapeeth et al. 2014). Insoluble oxalates cannot be measured by IC (Cheng et al. 2016) and Raman spectroscopy is only suitable to quantify insoluble oxalates at high concentrations (Carmona, Bellanato, and Escolar 1997; Chiu et al. 2010; Khalil and Azooz 2007). Other techniques (HPLC, enzyme assays, electrochemical techniques) were not designed for clay mineral sample analysis, or the procedures are time-consuming, yield inconsistent results or require addition of Ca^{2+} to promote precipitation (Cailleau, Braissant, and Verrecchia 2011b; Certini, Corti, and Ugolini 2000; Liu et al. 2015; Misiewicz et al. 2023; Mujinya et al. 2011; Shen et al. 2021; Vasant Naik Bharati Vidyapeeth et al. 2014). Liquid chromatography-mass spectrometry (LC-MS) may be considered the preferred choice among the existing technologies due to high sensitivity and precision (Elgstoen et al. 2010; Keevil and Thornton 2006; Misiewicz et al. 2023), but to our knowledge the technique has not been used for oxalate analysis of geological samples.

Infrared (IR) spectroscopy provides a potential solution to the problems of oxalate quantitation (Aleixandre-Tudo et al. 2018; Gobrecht, Roger, and Bellon-Maurel 2014). IR analysis has been shown to be more cost-effective compared to other techniques (Jozanikohan and Abarghooei 2022) and minimizes sample preparation and chemical waste, especially when an attenuated total reflectance (ATR) accessory is used (Aleixandre-Tudo et al. 2018; Bushong, Norman, and Slaton 2015; Mohamed et al. 2018; Pavia et al. 2015). IR spectroscopy is suitable for the analysis of heterogeneous samples when combined with chemometric techniques such as partial least-squares regression (PLSR) (Junaedi, Lestari, and Muchtaridi 2021b; Mohamed et al. 2018; Viscarra Rossel et al. 2006). Wavenumbers of absorption peaks commonly associated with biominerals, which are mainly detected in the mid-IR (MIR: 2500–25 000 nm) region, are shown in Table 1. IR spectroscopy has been used for semi-quantitative (Petrova et al. 2019) and quantitative analysis (Lin et al. 2019; Möller, Gergeleit, and Schüller 1989; Oka, Koide, and Sonoda 1985; Volmer, De Vries, and Goldschmidt 2001) of calcium oxalate in kidney stones, but no IR models have been developed for accurate quantification of oxalate salts in clay minerals or oxalic acid in solution. The aim of this study is to develop an efficient method to quantify CaOx and NaOx in a soil clay mineral matrix and oxalic acid in solution by calibrating

Table 1. Wavenumbers of IR absorption peaks associated with biominerals CaOx monohydrate (COM), CaOx dihydrate (COD) and NaOx.

Wavenumber (cm ⁻¹)	Functional group	Component	Reference
418	metal-O	NaOx	(Parekh et al. 2008)
515	C = O plane bend/Ca-O	Oxalate	(Bhatt and Paul 2008; Kachkoul et al. 2020)
610	metal-O	COD, NaOx	(Lin et al. 2019; Liu et al. 2020; Parekh et al. 2008)
650–670	C = O	COM	(Kachkoul et al. 2020; Lin et al. 2019; Liu et al. 2020; Modlin and Davies 1981)
750–780	C = O out-of-plane bend	COM	(Bhatt and Paul 2008; Chen, Sun, and Zhou 2013; Kachkoul et al. 2020; La Russa et al. 2009; Liu et al. 2020; Modlin and Davies 1981; Rojas-Molina et al. 2015; Sikka et al. 2008)
885	C-C	COM	(Lin et al. 2019; Liu et al. 2020; Modlin and Davies 1981; Parekh et al. 2008)
912		COD	(Lin et al. 2019; Liu et al. 2020)
947–960		COM	(Liu et al. 2020; Modlin and Davies 1981)
1000–1800	C-C	COM	(Lin et al. 2019; Parekh et al. 2008; Schmitt et al. 2018)
1250–1425	C-C	COM	(Parekh et al. 2008; Sikka et al. 2008)
1310–1330	C = O symmetric stretch	Oxalate	(Bhatt and Paul 2008; Chen, Sun, and Zhou 2013; Kachkoul et al. 2020; La Russa et al. 2009; Lin et al. 2019; Liu et al. 2020; Modlin and Davies 1981; Rojas-Molina et al. 2015; Schmitt et al. 2018)
1383	C = O symmetric stretch	Oxalate	(Kachkoul et al. 2020; Sikka et al. 2008)
1590–1620	C = O asymmetric stretch	COM	(Bhatt and Paul 2008; Echigo et al. 2005; Kachkoul et al. 2020; La Russa et al. 2009; Lin et al. 2019; Liu et al. 2020; Modlin and Davies 1981; Parekh et al. 2008; Rojas-Molina et al. 2015; Schmitt et al. 2018; Sikka et al. 2008)
1646	C = O	COD	(Kachkoul et al. 2020; Lin et al. 2019; Liu et al. 2020; Oyebiyi et al. 2018; Schmitt et al. 2018)
1660	C = O asymmetric stretch	Oxalate	(Bhatt and Paul 2008; Kachkoul et al. 2020; La Russa et al. 2009; Schmitt et al. 2018)
3286	O-H stretch (crystal H ₂ O)	COD	(Echigo et al. 2005; Kachkoul et al. 2020)
3400–3500	O-H stretch (crystal H ₂ O)	CaOx	(Bhatt and Paul 2008; Echigo et al. 2005; Kachkoul et al. 2020; Liu et al. 2020; Modlin and Davies 1981; Parekh et al. 2008; Schmitt et al. 2018)

models with chemical and spectral reference data of standards to predict concentrations of oxalate components by ATR-MIR analysis.

Materials and methods

An overview of the methods is presented in [Figure 1](#). The degree to which the samples for calibration of the MIR predictive model is representative of future datasets is of greater importance than the size of the chemical reference dataset (van Wyngaard et al. 2021). Our models were calibrated using a small but targeted reference dataset.

Sample collection and preparation

Clay mineral standards were prepared as mixtures ($n = 34$) consisting of minerals typically found in soils from a semi-arid region of South Africa where oxalate-rich vegetation occurs (Clarke et al. 2022; Francis 2008; Francis et al. 2013, 2015, 2020; Vermonti 2022). The standards consisted of soil clay minerals and oxalate salts at various concentrations (0–1.0 g g⁻¹ for CaOx and NaOx respectively) to test whether target analytes may be quantified reliably relative to other typical soil matrix components. The clay mineral mixtures were prepared by homogenizing milled analytical-grade calcium oxalate monohydrate (CaC₂O₄·H₂O, Thermo Scientific), sodium oxalate (Na₂C₂O₄, Sigma-Aldrich), calcium carbonate (CaCO₃, Sigma-Aldrich), gypsum (CaSO₄·2 H₂O, Kimix Chemical and Lab Supplies), quartz (SiO₂, Sigma-Aldrich) and kaolinite (KGa-1b from the Source Clay repository at Purdue University, USA) powders using a mortar and pestle. The

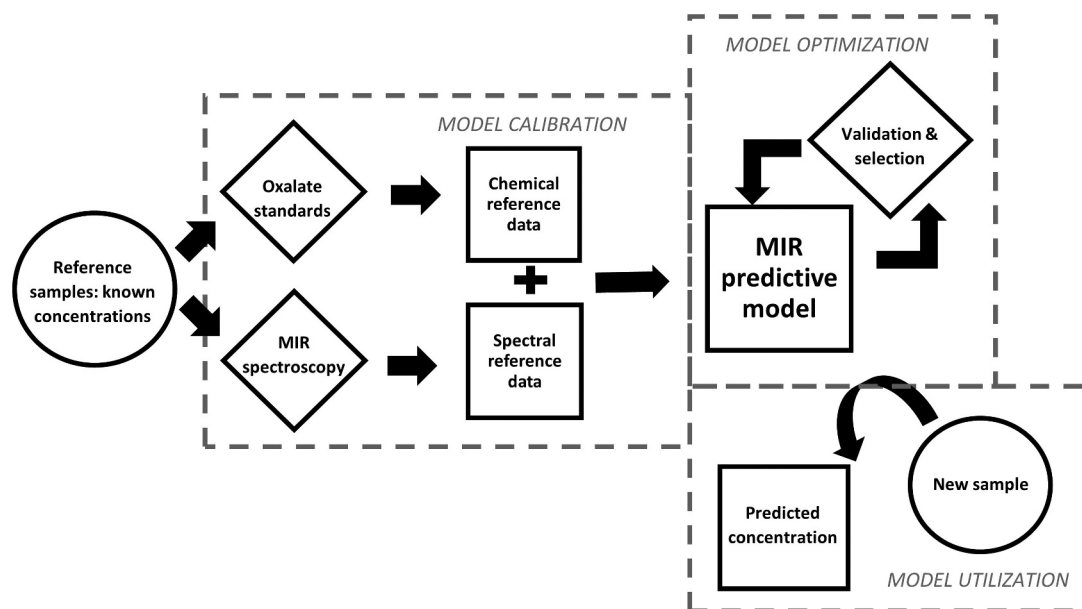


Figure 1. Flow chart showing overview of the development of a mid-infrared (MIR) spectroscopic technique to predict oxalate concentrations in new samples using only spectral information. The model is calibrated by correlation between oxalate concentrations and spectral data of a reference dataset. Several models may be developed due to different possible combinations of predictive model components; thus, the best-performing model is selected by validation procedures.

quantities of the components in each standard are given in [Table 2](#). Oxalic acid standards of various concentrations (0–0.01 M; $n = 32$) were prepared by dissolving analytical grade oxalic acid dihydrate (Merck) in water. The quantities of components in standard solutions are given in [Table 2](#).

Infrared spectroscopic modelling

IR model calibration

Spectral measurements of all solid and liquid samples were taken with an Alpha spectrometer (Bruker Optik, Ettlingen, Germany) operating in absorbance mode. A small quantity of each sample (~1 mL or equivalent mass of solid) was placed directly onto the ATR crystal surface of the MIR instrument. For solid samples, the probe was adjusted to make firm contact with the sample, while liquid samples were injected with a syringe via a sealed compartment. Sixty-four scans were collected in the range 350–7500 cm^{-1} at a resolution of 4 cm^{-1} .

MIR spectral-based models were calibrated using reference data derived from known theoretical concentrations of prepared oxalic acid solutions and clay mineral standards. Triplicate spectral scans of two standards (one clay mineral mixture as well as an oxalic acid solution) were included to incorporate spectral variability due to scattering of IR radiation by sample matrices (Alexandre-Tudo, Nieuwoudt, and du Toit 2019; Nel, Clarke, and Hardie 2023). Multivariate analyses were conducted using OPUS 8.2 (Independent JPEG Group 2018). Models predicting oxalate components based on sample spectral measurements were calibrated by correlating IR spectroscopic data to corresponding reference data using a PLSR algorithm (Mohamed et al. 2018; Nel, Clarke, and Hardie 2023) with the QUANT2 function in OPUS 8.2 (Independent JPEG Group 2018) software. The oxalate components predicted by the models were CaOx and NaOx in solid clay samples and oxalic acid in standard solutions.

Table 2. Composition of standard mineral mixtures and oxalic acid solutions.

Mineral (g g ⁻¹)						Solution (M)
CaOx [CaC ₂ O ₄ · H ₂ O]	NaOx [Na ₂ C ₂ O ₄]	CaCO ₃	CaSO ₄	Kaolinite	SiO ₂	Oxalic acid
0.000	0.615	0.000	0.000	0.385	0.000	0
0.027	0.580	0.000	0.002	0.370	0.020	0.0003
0.037	0.523	0.044	0.002	0.333	0.061	0.0006
0.051	0.494	0.070	0.006	0.315	0.064	0.0009
0.065	0.455	0.087	0.006	0.295	0.093	0.001
0.084	0.424	0.115	0.006	0.269	0.102	0.0013
0.097	0.395	0.126	0.007	0.252	0.122	0.0016
0.109	0.367	0.145	0.008	0.236	0.134	0.002
0.123	0.347	0.148	0.008	0.213	0.160	0.0023
0.132	0.324	0.160	0.009	0.209	0.166	0.0026
0.142	0.299	0.178	0.008	0.191	0.181	0.003
0.153	0.282	0.182	0.011	0.170	0.202	0.0033
0.161	0.259	0.195	0.012	0.166	0.207	0.0036
0.164	0.231	0.221	0.013	0.153	0.217	0.004
0.180	0.212	0.232	0.014	0.135	0.226	0.0043
0.182	0.200	0.241	0.014	0.127	0.237	0.0046
0.195	0.178	0.246	0.015	0.115	0.252	0.005
0.196	0.168	0.252	0.016	0.109	0.259	0.0053
0.207	0.150	0.262	0.016	0.098	0.268	0.0056
0.218	0.138	0.267	0.016	0.090	0.271	0.006
0.224	0.125	0.277	0.017	0.077	0.280	0.0063
0.226	0.109	0.288	0.017	0.065	0.295	0.0066
0.235	0.095	0.294	0.018	0.060	0.297	0.007
0.236	0.087	0.302	0.019	0.051	0.304	0.0073
0.243	0.071	0.311	0.019	0.045	0.311	0.0076
0.246	0.060	0.314	0.020	0.034	0.325	0.008
0.254	0.041	0.321	0.020	0.031	0.332	0.0083
0.253	0.038	0.329	0.019	0.028	0.332	0.0086
0.259	0.031	0.337	0.019	0.018	0.335	0.009
0.265	0.018	0.345	0.020	0.010	0.342	0.0093
0.270	0.013	0.350	0.021	0.006	0.341	0.0096
0.272	0.000	0.355	0.021	0.000	0.352	0.01
0.531	0.000	0.000	0.000	0.469	0.000	
1.000	0.000	0.000	0.000	0.000	0.000	
0.000	1.000	0.000	0.000	0.000	0.000	
0.000	0.000	0.000	0.000	0.000	1.000	
0.000	0.000	0.000	0.000	1.000	0.000	
0.000	0.000	0.000	1.000	0.000	0.000	
0.000	0.000	1.000	0.000	0.000	0.000	
0.000	0.000	1.000	0.000	0.000	0.000	
0.208	0.201	0.000	0.000	0.000	0.592	

The optimization procedure selected models with a combination of spectral pre-processing options with the lowest root mean square error of prediction (RMSEP)-values and a rank value <10 to ensure model parsimony (Pasquini 2018). The pre-processing techniques correct for baseline drift and light scattering (Lin et al. 2017; Nel, Clarke, and Hardie 2023). The best-performing model for prediction of each component of interest in the sample matrices analyzed in this study was reported in addition to figures of merit.

IR model validation

Validation was performed using the QUANT2 function in OPUS 8.2 (Independent JPEG Group 2018). Calibration and test set samples were selected using the Kennard-Stone algorithm, which allocates samples according to desired proportions such that similar distributions of the property of interest are obtained in sample calibration and validation subsets (Ramirez-Lopez and Stevens 2020). Outliers were automatically detected according to the Mahalanobis distance (Kotu and Deshpande 2019) and metrics of models with lower RMSEP after exclusion of outliers were

reported (<10% of original dataset). The ratio of performance to inter-quartile distance (RPIQ)-value of each model in this report was calculated using the yardstick package (Kuhn and Vaughan 2020) in the RStudio 1.2.5033 computing environment (RStudio Team 2019). The RPIQ-value is an IR model performance metric like the ratio of performance to deviation (RPD) metric, but accounts for log-normal distribution of data often encountered in biological datasets (Johnson et al. 2019). RPD is calculated as follows:

$$\text{RPD} = \frac{SD}{RMSE} \quad 1$$

where SD = standard deviation of the calibration/validation sample set (for $\text{RPD}_{\text{cal}}/\text{RPD}_{\text{val}}$ respectively)

$\text{RMSE} = \text{RMSECV}/\text{RMSEP}$ (for $\text{RPD}_{\text{cal}}/\text{RPD}_{\text{val}}$ respectively) (Alexandre-Tudo et al. 2018)

RPIQ is calculated similarly to RPD, by replacing SD with inter-quartile distance (Bellon-Maurel et al. 2010).

The Quant2 Analysis function in OPUS 8.2 (Independent JPEG Group 2018) software was used to assess the reproducibility of spectral measurements of solid and liquid samples. This was achieved by applying the developed models for prediction of CaOx and NaOx content (g g^{-1}) of a prepared mineral standard scanned in triplicate with the MIR instrument (repeat analyses of single sample) and calculating the degree of variability between replicates expressed as the coefficient of variation percentage (CV%). The models were also applied to predict oxalic acid concentration (M) of one oxalic acid standard scanned in triplicate with the IR spectrometer.

Results

Infrared spectroscopic analyses

The CV% values of MIR model-predicted oxalate salt components of the clay mineral standard (repeated scans of individual sample) were 1.1% and 0.5% for CaOx and NaOx, respectively. The CV% values of predicted oxalic acid concentration in the standard solution were 5.7%. Raw MIR spectra of an oxalic acid solution standard is shown in Figure 2. The absorption peaks

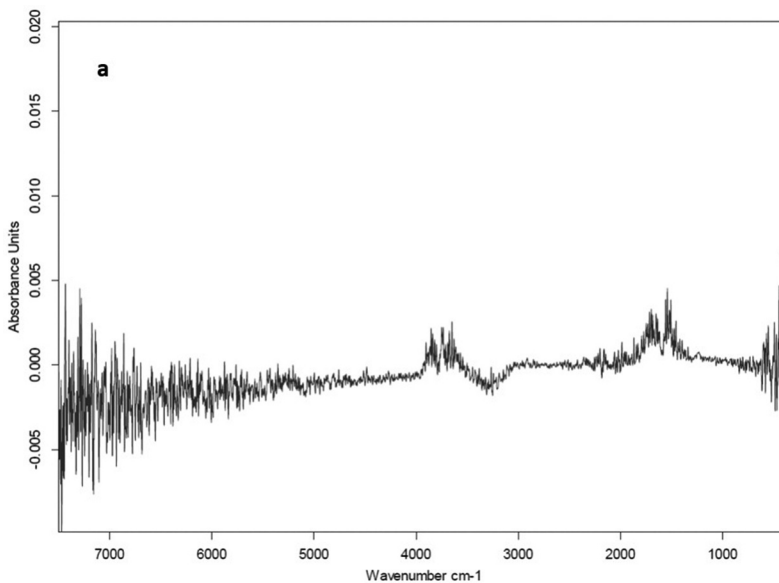


Figure 2. Unprocessed mid-infrared spectra of 0.01 M oxalic acid.

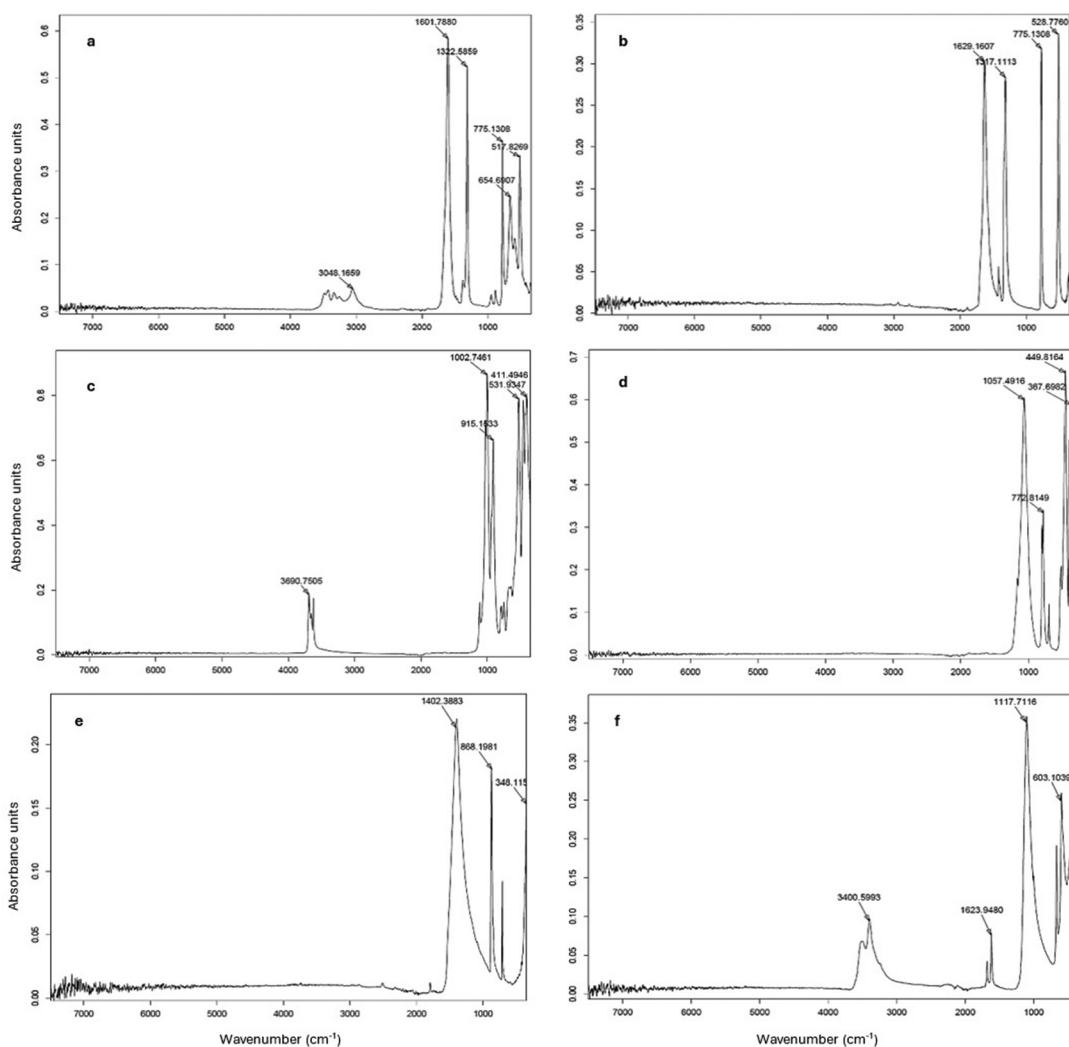


Figure 3. Unprocessed mid-infrared spectra pure solid minerals: calcium oxalate (CaOx, a), sodium oxalate (NaOx, b), kaolinite (c), SiO₂ (d), CaCO₃ (e) and CaSO₄ (f).

correspond to absorption of infrared radiation by hydroxyl (O-H, 3500–3700 cm⁻¹) and carboxyl (C=O, 1680–1720 cm⁻¹) functional groups (see Table 1). The MIR spectra of pure individual minerals used as components of clay standard mixtures are shown in Figure 3. The spectra show well-defined peaks corresponding to absorptions by carboxyl (655, 775, 1317, 1323, 1601 and 1630 cm⁻¹) and metal-O (517 and 528 cm⁻¹) functional groups of oxalate compounds (see Table 1). Crystal water O-H (3048, 3690 and 3401 cm⁻¹) groups may be associated with hydrated metal oxalate compounds (see Table 1), kaolinite (Saikia and Parthasarathy 2010) and gypsum (Dabbas, Eisa, and Kadhim 2013). The Si-O stretching (1057, 1003 and 773 cm⁻¹) and bending (449 and 411 cm⁻¹) modes are visible in the pure quartz as well as kaolinite spectra (Tran et al. 2013). The peak at 531 cm⁻¹ in pure kaolinite may be attributed to the Fe-O or Si-O-Al stretching mode, and absorption at 915 cm⁻¹ corresponds with OH deformation linked to Al (Saikia and Parthasarathy 2010). The pure gypsum spectrum shows S-O stretching

Table 3. Figures of merit for models predicting oxalate components in solid and liquid matrices based on MIR spectra of samples.

Component	Units	Matrix	R ²	RMSEP	RMSEP _{norm}	RPD	RPIQ	Rank	Wavelength regions (cm ⁻¹)	Pre-processing ⁱ	n ⁱⁱ	Cal: val ⁱⁱⁱ
CaOx	mmol g ⁻¹	Mineral standard	0.98	0.217	0.02	7.38	5.69	7	7497.9–6781.3209.3–2492.41779.7–1062.9	MSC	42	2: 1
NaOx	mmol g ⁻¹	Mineral standard	0.99	0.835	0.04	9.05	13.4	5	6068.3–3922.3209.3–1777.7	SNV	42	2: 1
Oxalic acid	M	H ₂ O standard	0.96	0.001	0.06	2.67	7.47	3	1779.7–1062.9	None	34	1: 2

ⁱSpectral data pre-processing methods include first and second derivative (1st and 2nd der.), constant offset elimination (COE), straight line subtraction (SLS), vector normalization (SNV) and multiplicative-scattering correction (MSC).

ⁱⁱn = Total number of samples for calibration and validation, including triplicate values of a single random sample for each of the prepared mineral mixtures and oxalic acid solution standards.

ⁱⁱⁱCal: val = calibration: validation sample splitting. A Kennard-Stone algorithm was used to split calibration and validation sample subsets such that both subsets included similar distributions of the measured component.

(1118 cm⁻¹) and bending (603 cm⁻¹) modes of the sulfate ion, while pure carbonate exhibits the stretching (1402 cm⁻¹) and bending (868 cm⁻¹) modes of the carbonyl functional group (Dabbas, Eisa, and Kadhim 2013).

Predictive model performance

Figures of merit for models predicting oxalate components in different matrices based on MIR spectra of samples are shown in Table 3. Validation graphs of these models for each oxalate component are illustrated in Figures 4 and 5. A very strong correlation exists between values predicted by spectral components and the true values of the measured property for all models (R² = 0.96, 0.98 and 0.99 for oxalic acid in solution, NaOx and CaOx in clay mineral mixtures). The RPD-values of models were larger than 2.0 (Table 3). Most RPIQ-values are higher than corresponding RPD values.

There are no absolute values of RMSEP that may be used as recommended thresholds of quantitative model accuracy, as RMSEP is reported in the same units as the target component measured. It is reasonable to assume that RMSEP smaller than 10% of the range of the component is indicative of relatively good predictive accuracy (Alexander, Tropsha, and Winkler 2015). Therefore, we judge models with RMSEP/range <0.1 to be suitably accurate for quantitative analysis of the measured property in this study. We define the RMSEP_{norm} as the normalized RMSEP, which is equivalent to the RMSEP/range value. Models for prediction of CaOx as well as NaOx in standard mineral mixtures have RMSEP_{norm} values <0.1 (Table 3). Models predicting oxalate anions in standard solutions have RMSEP_{norm} values <0.1 (see Table 3).

Discussion

We observed low CV% (<5%) of CaOx and NaOx predictions in replicate IR measurements of the solid standard, which confirms excellent reproducibility of oxalate salts in a clay mineral mixture (Gomez and Gomez 1984). Relatively low CV% (<6%) in replicate IR measurements of the oxalic acid standard shows good reproducibility of spectral measurements of a liquid sample. The better reproducibility of MIR model predictions is attributed to spectral pre-processing procedures, as well as homogeneity of milled mineral samples, which reduces additive scatter of radiation by solid particulate solids (Naes et al. 2002). Excellent correlation between true and predicted CaOx and NaOx concentrations in compound clay mineral standards matches is equivalent to that obtained by IR analysis of CaOx in mineral mixtures with composition like that of human kidney stones

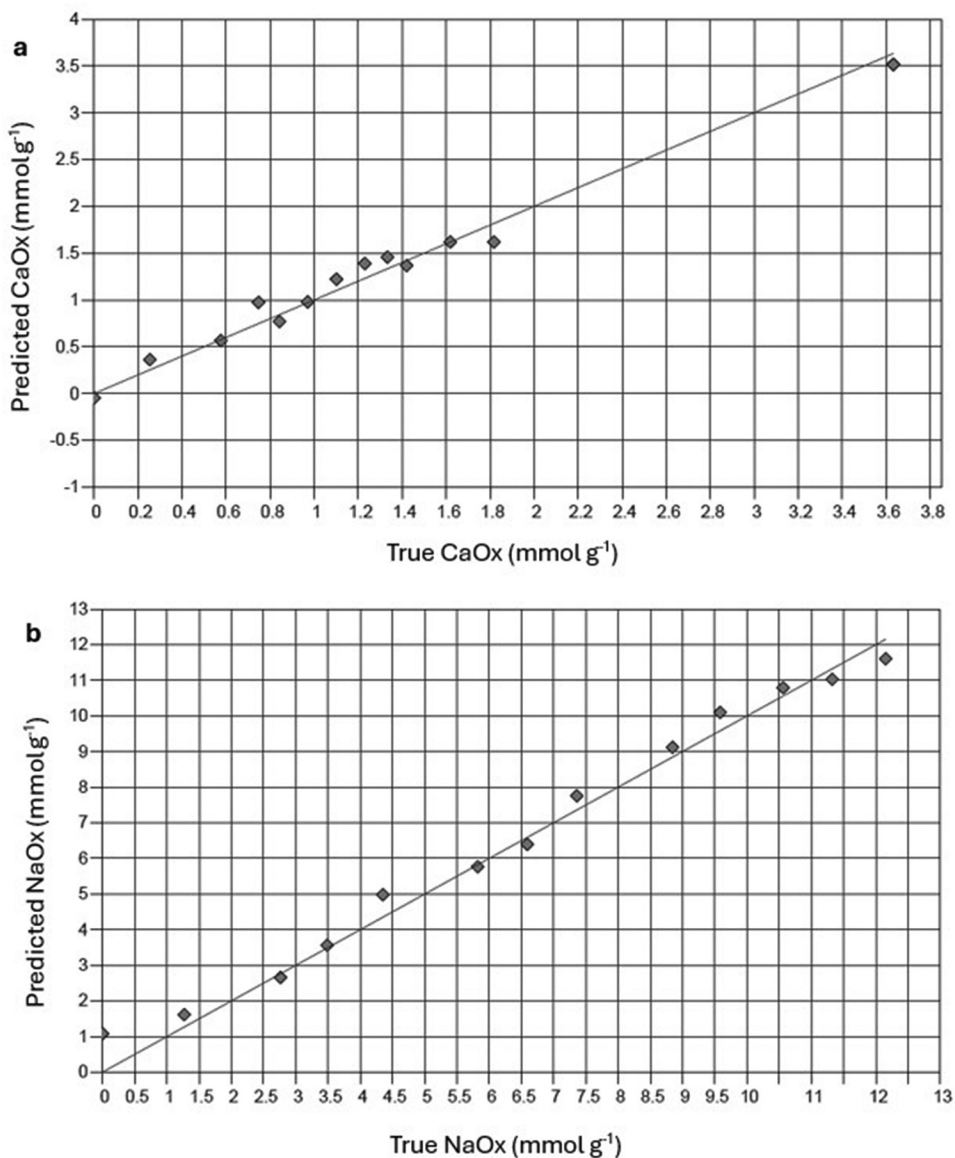


Figure 4. Plots for validation of infrared spectral-based models to determine concentrations of (a) calcium oxalate, CaOx and (b) sodium oxalate, NaOx in prepared mineral mixtures. Solid line represents $y = x$ reference line.

($R^2 \geq 0.98$) (Volmer et al. 1993). The IR models show slightly better fit than models that estimate the ratio of CaOx monohydrate to dihydrate in artificial mineral mixtures (Lin et al. 2019; Oka, Koide, and Sonoda 1985).

Wavelength regions selected by MIR spectral-based models to predict oxalate components in solid and liquid samples (Table 3) were mainly representative of carboxylic acid and crystal hydration functional groups. The “noise” observed closer to the further ends of the spectrum (Figures 2 and 3) contributes less meaningful information to models, which explains preclusion of these regions as predictive components by the PLSR algorithm. The carboxyl absorption at 655 cm^{-1} and crystal water absorptions between 3000 and 3500 cm^{-1} (Figure 3) is unique to the pure CaOx spectrum, creating a visible distinction between the metal oxalate salts. The 660 cm^{-1} peak is

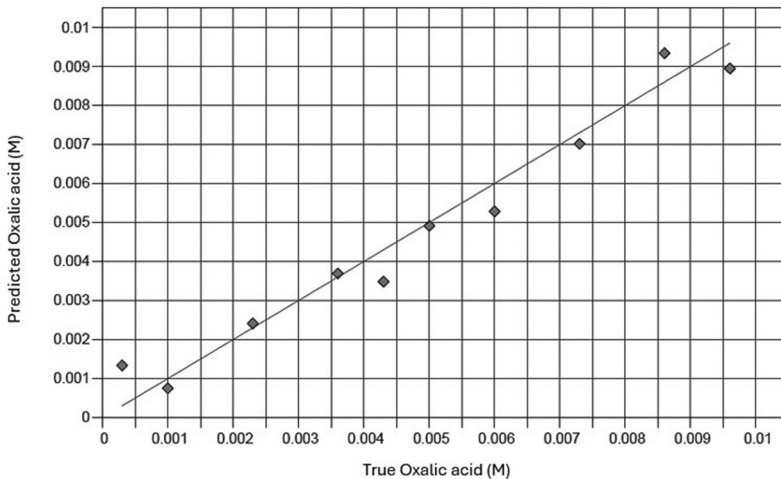


Figure 5. Plots for validation of infrared spectral-based models to determine concentrations of oxalic acid in a standard solution. Solid line represents $y = x$ reference line.

a characteristic feature of CaOx that can be used to distinguish the monohydrate from the dihydrate form (Lin et al. 2019; Oka, Koide, and Sonoda 1985). Possibilities of overlapping peaks in mixed samples include the S-O bending mode of gypsum and carboxyl absorption of CaOx (603 cm^{-1} and 655 cm^{-1}), crystal hydration waters of CaOx monohydrate, kaolinite, and gypsum (3048 , 3690 and 3401 cm^{-1}), and Si-O stretching of silica and carboxyl of carboxyl absorptions by oxalates (773 cm^{-1} and 775 cm^{-1}). A slight overlap may also exist between the carbonyl group of carbonate (1402 cm^{-1}) and the carboxyl absorptions of oxalates ($1300\text{--}1600\text{ cm}^{-1}$, Figure 3). Differences between wavelength regions used as predictive components by models for quantification of CaOx and NaOx (Table 3) show the capacity of the models to distinguish between the target analytes in compound materials based on absorptions in specific IR wavelength regions. This confirms the specificity of the IR technique for analyses of both CaOx and water-soluble oxalates in soil clay mineral mixtures.

The RPD and RPIQ of all models were greater than 2.0 (Table 3) which indicates reliable model performance (Bellon-Maurel et al. 2010). Low $\text{RMSEP}_{\text{norm}}$ values of models ($\text{RMSEP}_{\text{norm}} < 0.05$ for prediction of CaOx and NaOx; Table 3) confirm the accuracy of MIR spectroscopy to quantify oxalate salts in clay mineral mixtures. This level of accuracy was also achieved for IR analysis of CaOx in artificial mineral mixtures that mimic composition of human kidney stones (Volmer et al. 1993). Oxalic acid concentrations in solution were also predicted with good accuracy ($\text{RMSEP}_{\text{norm}} = 0.06$, Table 3). These results provide evidence of the potential for MIR spectroscopy to be applied in quantitative studies of oxalate dynamics in soils. This technique should be tested in future on mineral samples that contain organic matter, which are more complex than pure mineral mixtures.

Conclusions

This work demonstrates that MIR spectroscopic analysis in conjunction with chemometric data processing can be used to differentiate between soluble and insoluble oxalates in heterogeneous inorganic materials. To our knowledge, this is the first report of MIR spectral-based models to determine soluble and sparingly soluble oxalate salt concentrations in soil clay mineral mixtures and oxalic acid in solution. Our MIR models reliably quantify both CaOx and NaOx concentrations in compound clay mineral standards and oxalic acid in aqueous solution. We suggest that MIR

spectroscopy is a more efficient and cost-effective alternative to chemical methods of total and water-soluble oxalate salt quantification in geological samples.

Acknowledgement

We thank the Stellenbosch University Postgraduate Office and The Skye Foundation for bursary provision. This material is based upon work supported by the National Science Foundation (USA) under Grants No 2224993 and No 2224994 and the National Research Foundation of South Africa (Grant Number 150452) as part of the Biodiversity on a Changing Planet program. We would also like to acknowledge Janine Colling and the DSI-BIOGRIP soil biogeochemistry node for time spent on ion chromatography method development.

Disclosure statement

No potential conflict of interest was reported by the author(s).

Funding

The work was supported by the National Science Foundation and National Research Foundation of South Africa [2224993 and 150452 respectively].

References

- Alexandre-Tudo, J. L., H. Nieuwoudt, and W. du Toit. 2019. Towards on-line monitoring of phenolic content in red wine grapes: A feasibility study. *Food Chemistry* 270:322–31. doi:10.1016/j.foodchem.2018.07.118.
- Alexandre-Tudo, J. L., H. Nieuwoudt, A. Olivieri, J. L. Alexandre, and W. du Toit. 2018. Phenolic profiling of grapes, fermenting samples and wines using UV-Visible spectroscopy with chemometrics. *Food Control* 85:11–22. doi:10.1016/j.foodcont.2017.09.014.
- Alexander, D. L. J., A. Tropsha, and D. A. Winkler. 2015. Beware of R2: Simple, unambiguous assessment of the prediction accuracy of QSAR and QSPR models. *Journal of Chemical Information and Modeling* 55 (7):1316–22. doi:10.1021/acs.jcim.5b00206.
- Arnott, H. J., and M. A. Webb. 2013. Twinned raphides of calcium oxalate in grape (vitis): Implications for crystal stability and function. *International Journal of Plant Sciences* 161 (1):133–42. doi:10.1086/314230.
- Bailey, S. W., D. C. Buso, and G. E. Likens. 2003. Implications of sodium mass balance for interpreting the calcium cycle of a forested ecosystem. *Ecology* 84 (2):471–84. doi:10.1890/0012-9658(2003)084[0471:IOSMBF]2.0.CO;2.
- Bellon-Maurel, V., E. Fernandez-Ahumada, B. Palagos, J. M. Roger, and A. McBratney. 2010. Critical review of chemometric indicators commonly used for assessing the quality of the prediction of soil attributes by NIR spectroscopy. *TrAC Trends in Analytical Chemistry* 29 (9):1073–81. doi:10.1016/j.trac.2010.05.006.
- Bhatt, P. A., and P. Paul. 2008. Analysis of urinary stone constituents using powder X-ray diffraction and FT-IR. *Journal of Chemical Sciences* 120 (2):267–73. doi:10.1007/s12039-008-0032-1.
- Braissant, O., G. Cailleau, M. Aragno, and E. P. Verrecchia. 2004. Biologically induced mineralization in the tree milicia excelsa (Moraceae): Its causes and consequences to the environment. *Geobiology* 2 (1):59–66. doi:10.1111/j.1472-4677.2004.00019.x.
- Braissant, O., E. P. Verrecchia, and M. Aragno. 2002. Is the contribution of bacteria to terrestrial carbon budget greatly underestimated? *Naturwissenschaften* 89 (8):366–70. doi:10.1007/s00114-002-0340-0.
- Bushong, J. T., R. J. Norman, and N. A. Slaton. 2015. Near-infrared reflectance spectroscopy as a method for determining organic carbon concentrations in soil. *Communications in Soil Science & Plant Analysis* 46 (14):1791–801. doi:10.1080/00103624.2015.1048250.
- Cailleau, G., O. Braissant, and E. P. Verrecchia. 2011a. Turning sunlight into stone: The oxalate-carbonate pathway in a tropical tree ecosystem. *Biogeosciences* 8 (7):1755–67. doi:10.5194/bg-8-1755-2011.
- Cailleau, G., O. Braissant, and E. P. Verrecchia. 2011b. Turning sunlight into stone: The oxalate-carbonate pathway in a tropical tree ecosystem. *Biogeosciences* 8 (7):1755–67. doi:10.5194/bg-8-1755-2011.
- Cailleau, G., M. Mota, S. Bindschedler, P. Junier, and E. P. Verrecchia. 2014. Detection of active oxalate-carbonate pathway ecosystems in the Amazon Basin: Global implications of a natural potential C sink. *Catena* 116:132–41. doi:10.1016/j.catena.2013.12.017.
- Carmona, P., J. Bellanato, and E. Escolar. 1997. Infrared and Raman spectroscopy of urinary calculi: A review. *Biospectroscopy* 3 (5):331–46. doi:10.1002/(SICI)1520-6343(1997)3:5<331:AID-BSPY2>3.0.CO;2-5.

- Certini, G., G. Corti, and F. C. Ugolini. 2000. Vertical trends of oxalate concentration in two soils under abies alba from Tuscany (Italy). *Journal of Plant Nutrition and Soil Science* 163 (2):173–77. doi:10.1002/(SICI)1522-2624(200004)163:2<173:AID-JPLN173>3.0.CO;2-H.
- Cheng, Z. Y., D. C. Fernández-Remolar, M. R. M. Izawa, D. M. Applin, M. Chong Díaz, M. Fernandez-Sampedro, M. García-Villadangos, T. Huang, L. Xiao, V. Parro, et al. 2016. Oxalate formation under the hyperarid conditions of the atacama desert as a mineral marker to provide clues to the source of organic carbon on mars. *Journal of Geophysical Research: Biogeosciences* 121(6):1593–604. doi:10.1002/2016JG003439.
- Chen, J., S. Sun, and Q. Zhou. 2013. Direct observation of bulk and surface chemical morphologies of ginkgo biloba leaves by Fourier transform mid- and near-infrared microspectroscopic imaging. *Analytical and Bioanalytical Chemistry* 405 (29):9385–400. doi:10.1007/s00216-013-7366-3.
- Chiu, Y.-C., H.-Y. Yang, S.-H. Lu, and H. K. Chiang. 2010. Micro-Raman spectroscopy identification of urinary stone composition from ureteroscopic lithotripsy urine powder. *Journal of Raman Spectroscopy* 41 (2):136–41. doi:10.1002/jrs.2418.
- Clarke, C. E., M. Vermooten, A. Watson, M. Hattingh, J. A. Miller, and M. L. Francis. 2022. Downward migration of salts in termite-affected soils: Implications for groundwater salinization. *Geoderma* 413:115747. doi:10.1016/j.geoderma.2022.115747.
- Dabbas, M. A., M. Y. Eisa, and W. H. Kadhim. 2013. Estimation of gypsum- calcite percentages using a Fourier transform infrared spectrophotometer (FTIR), in Alexandria Gypsiferous Soil -Iraq. In 2nd international conference on IRAQI oil studies, 2013, University of Baghdad, Baghdad.
- Dauer, J. M., and S. S. Perakis. 2013. Contribution of calcium oxalate to soil-exchangeable calcium. *Soil Science* 178 (12):671–78. doi:10.1097/SS.0000000000000029.
- Dauer, J. M., and S. S. Perakis. 2014. Calcium oxalate contribution to calcium cycling in forests of contrasting nutrient status. *Forest Ecology and Management* 334:64–73. doi:10.1016/j.foreco.2014.08.029.
- Dutton, M. V., and C. S. Evans. 1996. Oxalate production by fungi: Its role in pathogenicity and ecology in the soil environment. *Canadian Journal of Microbiology* 42 (9):881–95. doi:10.1139/m96-114.
- Echigo, T., M. Kimata, A. Kyono, M. Shimizu, and T. Hatta. 2005. Re-investigation of the crystal structure of whewellite [Ca(c 2 O 4)-H 2 O] and the dehydration mechanism of caoxite [Ca(c 2 O 4)-3H 2 O]. *Mineralogical Magazine* 69 (1):77–88. doi:10.1180/0026461056910235.
- Elgstoen, K. B. P., B. Woldseth, K. Hoie, and L. Morkrid. 2010. Liquid chromatography-tandem mass spectrometry determination of oxalate in spot urine. *Scandinavian Journal of Clinical and Laboratory Investigation* 70 (3):145–50. doi:10.3109/00365510903578765.
- Franceschi, V. R., and H. T. Horner. 1980a. Calcium oxalate crystals in plants. *The Botanical Review* 46 (4):361–427. doi:10.1007/BF02860532.
- Franceschi, V. R., and H. T. Horner. 1980b. Calcium oxalate crystals in plants. *The Botanical Review* 46 (4):361–427. doi:10.1007/BF02860532.
- Francis, M. L. 2008. Soil Formation on the Namaqualand Coastal Plain. Stellenbosch: PhD thesis, Stellenbosch University. [Online]. <https://everythingcomputerscience.com/books/regmods.pdf/>.
- Francis, M. L., F. Ellis, J. J. N. Lambrechts, and R. M. Poch. 2013. A micromorphological view through a Namaqualand termitaria (Heuweltjie, a Mima-like mound). *Catena* 100 (February 2017):57–73. doi:10.1016/j.catena.2012.08.004.
- Francis, M. L., M. V. Fey, F. Ellis, and M. Poch. 2015. Horizontes petrodúricos e “petrosepiolíticos” em solos de Namaqualand, África do Sul. *Spanish Journal of Soil Science* 2 (1):8–25. doi:10.3232/SJSS.2012.V2.N1.01.
- Francis, M. L., T. O. Majodina, and C. E. Clarke. 2020. A geographic expression of the sepiolite-palygorskite continuum in soils of northwest South Africa. *Geoderma* 379:114615. doi:10.1016/j.geoderma.2020.114615.
- Francis, M. L., and R. M. Poch. 2019. Calcite accumulation in a South African heuweltjie: Role of the termite microhodotermes Viator and oribatid mites. *Journal of Arid Environments* 170:170. doi:10.1016/j.jaridenv.2019.05.009.
- Gobrecht, A., J. M. Roger, and V. Bellon-Maurel. 2014. Major issues of diffuse reflectance NIR spectroscopy in the specific context of soil carbon content estimation. *A Review Advances in Agronomy* 123:145–75.
- Gomez, K. A., and A. A. Gomez. 1984. *Statistical Procedures for Agricultural Research*. 2nd ed. New York: John Wiley & Sons, Inc.
- Graustein, W. C., C. Kermit Jr, and P. Sollins. 2011. Calcium oxalate: Occurrence in soils and effect on nutrient and geochemical cycles. *Advancement of Science* 198 (4323):1252–54. doi:10.1126/science.198.4323.1252.
- Hervé, V., A. Simon, F. Randevoison, G. Cailleau, G. Rajoelison, H. Razakamanarivo, S. Bindschedler, E. Verrecchia, and P. Junier. 2021. Functional diversity of the litter-associated fungi from an oxalate–carbonate pathway ecosystem in Madagascar. *Microorganisms [Internet]* 9 (5):1–12. doi:10.3390/microorganisms9050985.
- Hofmann, B. A., and S. M. Bernasconi. 1998. Review of occurrences and carbon isotope geochemistry of oxalate minerals: Implications for the origin and fate of oxalate in diagenetic and hydrothermal fluids. *Chemical Geology* 149 (1–2):127–46. doi:10.1016/S0009-2541(98)00043-6.
- Ilarslan, H., R. G. Palmer, J. Imsande, and H. T. Horner. 1997. Quantitative determination of calcium oxalate and oxalate in developing seeds of soybean (Leguminosae). *American Journal of Botany* 84 (8):1042–46. doi:10.2307/2446147.
- Independent JPEG Group. 2018. [Online]. Accessed August 8, 2023. <https://everythingcomputerscience.com/books/regmods.pdf/>.

- Jilling, A., M. Keiluweit, J. L. M. Gutknecht, and A. S. Grandy. 2021. Priming mechanisms providing plants and microbes access to mineral-associated organic matter. *Soil Biology and Biochemistry* 158:108265. doi:10.1016/j.soilbio.2021.108265.
- Johnson, J. M., E. Vandamme, K. Senthilkumar, A. Sila, K. D. Shepherd, and K. Saito. 2019. Near-infrared, mid-infrared or combined diffuse reflectance spectroscopy for assessing soil fertility in rice fields in sub-saharan Africa. *Geoderma* 354:354. doi:10.1016/j.geoderma.2019.06.043.
- Johnston, C. G., and J. R. Vestal. 1993. Biogeochemistry of oxalate in the Antarctic cryptoendolithic lichen-dominated community. *Microbial Ecology* 25 (3):305–19. doi:10.1007/BF00171895.
- Jozanikohan, G., and M. N. Abarghoeei. 2022. The Fourier transform infrared spectroscopy (FTIR) analysis for the clay mineralogy studies in a clastic reservoir. *Journal of Petroleum Exploration and Production Technology* 12 (8):2093–106. doi:10.1007/s13202-021-01449-y.
- Junaedi, E., K. Lestari, and M. Muchtaridi. 2021b. Infrared spectroscopy technique for quantification of compounds in plant-based medicine and supplement. *Journal of Advanced Pharmaceutical Technology and Research* 12 (1):1–7. doi:10.4103/japtr.JAPTR_96_20.
- Kachkoul, R., T. S. Houssaini, M. Mohim, R. El Habbani, and A. Lahrichi. 2020. Chemical compounds identification and antioxidant and calcium oxalate anticrystallization activities of punica granatum L. *Evidence-Based Complementary and Alternative Medicine* 2020:1–14. doi:10.1155/2020/9424510.
- Keevil, B. G., and S. Thornton. 2006. Quantification of urinary oxalate by liquid chromatography-tandem mass spectrometry with online weak anion exchange chromatography. *Clinical Chemistry* 52 (12):2294–96. doi:10.1373/clinchem.2006.075275.
- Khalil, S. K. H., and M. A. Azooz. 2007. Application of vibrational spectroscopy in identification of the composition of the urinary stones. *Journal of Applied Sciences Research* 3 (5):387–91.
- Kotani, A., H. Ishikawa, T. Shii, M. Kuroda, Y. Mimaki, K. Machida, K. Yamamoto, and H. Hakamata. 2023. Determination of oxalic acid in herbal medicines by semi-micro hydrophilic interaction liquid chromatography coupled with electrochemical detection. *Analytical Sciences* 39 (4):441–46. doi:10.1007/s44211-022-00245-w.
- Kotu, V., and B. Deshpande. 2019. Anomaly detection. In *Data Science*, eds. M. Kaufmann, 2nd, 447–65. Elsevier. doi:10.1016/B978-0-12-814761-0.00013-7.
- Krieger, C., C. Calvaruso, C. Morlot, S. Uroz, L. Salsi, and M. P. Turpault. 2017. Identification, distribution, and quantification of biominerals in a deciduous forest. *Geobiology* 15 (2):296–310. doi:10.1111/gbi.12223.
- Kuhn, M., and D. Vaughan & RStudio Team. 2020.
- La Russa, M. F., S. A. Ruffolo, G. Barone, G. M. Crisci, P. Mazzoleni, and A. Pezzino. 2009. The use of FTIR and micro-FTIR spectroscopy: An example of application to cultural heritage. *International Journal of Spectroscopy* 2009:1–5. doi:10.1155/2009/893528.
- Lin, M. H., Y. L. Song, P. A. Lo, C. Y. Hsu, A. T. L. Lin, E. Y. H. Huang, and H. K. Chiang. 2019. Quantitative analysis of calcium oxalate hydrate urinary stones using FTIR and 950/912 cm^{-1} peak ratio. *Vibrational Spectroscopy* 102:85–90. doi:10.1016/j.vibspec.2019.03.006.
- Lin, Z. D., Y. B. Wang, R. J. Wang, L. S. Wang, C. P. Lu, Z. Y. Zhang, L. T. Song, and Y. Liu. 2017. Improvements of the vis-NIRS model in the prediction of soil organic matter content using spectral pretreatments, sample selection, and wavelength optimization. *Journal of Applied Spectroscopy* 84 (3):529–34. doi:10.1007/s10812-017-0505-4.
- Liu, H., X. Y. Sun, F. X. Wang, and J. M. Ouyang. 2020. Regulation on calcium oxalate crystallization and protection on HK-2 cells of tea polysaccharides with different molecular weights. *Oxidative Medicine and Cellular Longevity* 2020:1–14. doi:10.1155/2020/5057123.
- Liu, Y., C. Zhang, B. Li, H. Li, and H. Zhan. 2015. Extraction and determination of total and soluble oxalate in pulping and papermaking raw materials. *BioRes* 10 (3):4580–87. doi:10.15376/biores.10.3.4580-4587.
- Martin, G., M. Guggiari, D. Bravo, J. Zopfi, G. Cailleau, M. Aragno, D. Job, E. Verrecchia, and P. Junier. 2012. Fungi, bacteria and soil pH the oxalate–carbonate pathway as a model for metabolic interaction. *Environmental Microbiology* 14 (11):2960–70. doi:10.1111/j.1462-2920.2012.02862.x.
- Misiewicz, B., D. Mencer, W. Terzaghi, and A. L. VanWert. 2023. Analytical methods for oxalate quantification: The ubiquitous organic anion. *Molecules* 28 (7):3206. doi:10.3390/molecules28073206.
- Modenesi, P., M. Piana, P. Giordani, A. Tafanelli, and A. Bartoli. 2000. Calcium oxalate and medullary architecture in *Xanthomaculina convoluta*. *Lichenologist (London, England)* 32 (5):505–12. doi:10.1006/lich.2000.0276.
- Modlin, M., and P. J. Davies. 1981. The composition of renal stones analysed by infrared spectroscopy. *South African Medical Journal* 59 (10):337–41.
- Mohamed, E. S., A. M. Saleh, A. B. Belal, and A. A. Gad. 2018. Application of near-infrared reflectance for quantitative assessment of soil properties. *The Egyptian Journal of Remote Sensing and Space Sciences* 21 (1):1–14. doi:10.1016/j.ejrs.2017.02.001.
- Möller, K., M. Gergeleit, and P. Schüller. 1989. Analysis of urinary stones by computerized infrared Spectroscopy1. *Clinical Chemistry and Laboratory Medicine* 27 (9):639–42. doi:10.1515/cclm.1989.27.9.639.
- Mujinya, B. B., F. Mees, P. Boeckx, S. Bodé, G. Baert, H. Erens, S. Delefortrie, A. Verdoodt, M. Ngongo, and E. Van Ranst. 2011. The origin of carbonates in termite mounds of the Lubumbashi area. *DR Congo Geoderma* 165 (1):95–105. doi:10.1016/j.geoderma.2011.07.009.

- Naes, T., T. Isaksson, T. Fearn, and T. Davies. 2002. *A user-friendly guide to multivariate calibration and classification*. Chichester: NIR Publications.
- Nakata, P. A. 2003. Advances in our understanding of calcium oxalate crystal formation and function in plants. *Plant Science* 164 (6):901–09. doi:10.1016/S0168-9452(03)00120-1.
- Nel, T., C. E. Clarke, and A. G. Hardie. 2023. Comparison of soil pH and exchangeable cation quantification by various wet methods with near- and mid-infrared spectroscopy prediction. *Communications in Soil Science and Plant Analysis* 54 (17):2425–38. doi:10.1080/00103624.2023.2223657.
- Oka, T., T. Koide, and T. Sonoda. 1985. Estimation by infrared spectrophotometer of the calcium oxalate dihydrate to calcium oxalate monohydrate ratio. *Journal of Urology* 134 (4):813–17. doi:10.1016/S0022-5347(17)47445-3.
- Oyebiyi, O. O., J. O. Ojetade, S. A. Muda, and A. A. Amusan. 2018. Comparative study of three methods of determining cation exchange capacity of three major soils in the rainforest region of Southwestern Nigeria. *Communications in Soil Science and Plant Analysis* 49 (18):2338–44. doi:10.1080/00103624.2018.1499768.
- Pantigoso, H. A., Y. He, M. J. DiLegge, and J. M. Vivanco. 2021. *Methods for root exudate collection and analysis*. eds. L. Carvalhais & P. Dennis. 291–303. New York: Humana Press *Methods in Molecular Biology*.
- Parekh, B. B., P. M. Vyas, S. R. Vasant, and M. J. Joshi. 2008. Thermal, FT-IR and dielectric studies of gel grown sodium oxalate single crystals. *Bulletin of Materials Science* 31 (2):143–47. doi:10.1007/s12034-008-0025-1.
- Pasquini, C. 2018. Near infrared spectroscopy: A mature analytical technique with new perspectives – a review. *Analytica chimica acta* 1026:8–36. doi:10.1016/j.aca.2018.04.004.
- Pavia, D. L., G. M. Lampman, G. S. Kriz, and J. R. Vyvyan. 2015. *Infrared Spectroscopy*. 5th ed. Bellingham, Washington: Cengage Learning *Introduction to Spectroscopy*.
- Petrova, D., K. Petkova, I. Saltirov, and T. S. Kolev. 2019. Application of vibrational spectroscopy and XRD analysis for investigation of calcium oxalate kidney stones. *Bulgarian Chemical Communications* 51 (1):88–95.
- Pons, S., S. Bindschedler, D. Sebag, P. Junier, E. Verrecchia, and G. Cailleau. 2018. Biocontrolled soil nutrient distribution under the influence of an oxalogenic-oxalotrophic ecosystem. *Plant and Soil* 425 (1–2):145–60. doi:10.1007/s11104-018-3573-1.
- Pylro, V. S., A. L. M. de Freitas, W. C. Otoni, I. R. da Silva, A. C. Borges, M. D. Costa, and A. Guerrero-Hernandez. 2013. Calcium oxalate crystals in eucalypt ectomycorrhizae: Morphochemical characterization. *Public Library of Science ONE* 8 (7):e67685. doi:10.1371/journal.pone.0067685.
- Ramirez-Lopez, L., and A. Stevens. 2020. kenStone: Kennard-Stone algorithm for calibration sampling. [Online] Accessed September 28, 2020. <https://everythingcomputerscience.com/books/regmods/pdf/>.
- Rehman, H. U., R. M. Poch, F. Scarciglia, and M. L. Francis. 2021. A carbon-sink in a sacred forest: Biologically-driven calcite formation in highly weathered soils in Northern Togo (West Africa). *Catena* 198 (November 2020):105027. doi:10.1016/j.catena.2020.105027.
- Rojas-Molina, I., E. Gutiérrez-Cortez, M. Bah, A. Rojas-Molina, C. Ibarra-Alvarado, E. Rivera-Muñoz, A. Del Real, and M. D. L. A. Aguilera-Barreiro. 2015. Characterization of calcium compounds in *Opuntia ficus indica* as a source of calcium for human diet. *Journal of Chemistry* 2015:1–8. doi:10.1155/2015/710328.
- Ross, A. B., G. P. Savage, R. J. Martin, and L. Vanhanen. 1999. Oxalates in oca (New Zealand yam) (*Oxalis tuberosa* mol.). *Journal of Agricultural and Food Chemistry* 47 (12):5019–22. doi:10.1021/jf990332r.
- Rowley, M. C., H. Estrada-Medina, M. Tzec-Gamboa, A. Rozin, G. Cailleau, E. P. Verrecchia, and I. Green. 2017. Moving carbon between spheres, the potential oxalate-carbonate pathway of *Brosimum alicastrum* Sw.; moraceae. *Plant and Soil* 412 (1–2):465–79. doi:10.1007/s11104-016-3135-3.
- RStudio Team. 2019. [Online]. <https://everythingcomputerscience.com/books/regmods/pdf/>.
- Saikia, B. J., and G. Parthasarathy. 2010. Fourier transform infrared spectroscopic characterization of kaolinite from Assam and Meghalaya, Northeastern India. *Journal of Modern Physics* 1 (04):206–10. doi:10.4236/jmp.2010.14031.
- Schmitt, A. D., N. Borrelli, D. Ertlen, S. Gangloff, F. Chabaux, and M. Osterrieth. 2018. Stable calcium isotope speciation and calcium oxalate production within beech tree (*Fagus sylvatica* L.) organs. *Biogeochemistry* 137 (1–2):197–217. doi:10.1007/s10533-017-0411-0.
- Shen, Y., X. Luo, H. Li, Q. Guan, and L. Cheng. 2021. Evaluation of a high-performance liquid chromatography method for urinary oxalate determination and investigation regarding the pediatric reference interval of spot urinary oxalate to creatinine ratio for screening of primary hyperoxaluria. *Journal of Clinical Laboratory Analysis* 35 (8):1–9. doi:10.1002/jcla.23870.
- Sikka, S., C. Selwitz, E. Doehne, G. Chiari, and H. Khanjian. 2008. Presentation for the paper: Qualitative and quantitative methods of detection and mapping of “calcium oxalate deposits” on treated limestones and marbles. Presentation at: Stone consolidation in cultural heritage : research and practice : proceedings of the international symposium. Lisbon 6-7 May, 2008. (December 2017):445–54.
- Tooulakou, G., A. Giannopoulos, D. Nikolopoulos, P. Bresta, E. Dotsika, M. G. Orkoulas, C. G. Kontoyannis, C. Fasseas, G. Liakopoulos, M. I. Klapa, et al. 2016. Alarm photosynthesis: Calcium oxalate crystals as an internal CO₂ source in plants. *Plant Physiology* 171(4):2577–85. doi:10.1104/pp.16.00111.
- Tran, T. N., T. V. A. Pham, M. L. P. Le, T. P. T. Nguyen, and V. M. Tran. 2013. Synthesis of amorphous silica and sulfonic acid functionalized silica used as reinforced phase for polymer electrolyte membrane. *Advances in Natural Sciences: Nanoscience and Nanotechnology* 4 (4):045007. doi:10.1088/2043-6262/4/4/045007.

- Uren, N. C. 2018. Calcium oxalate in soils, its origins and fate – a review. *Soil Research* 56 (5):443–50. doi:10.1071/SR17244.
- van Wyngaard, E., E. Blancquaert, H. Nieuwoudt, and A.-T. Jose Luis. 2021. Infrared spectroscopy and chemometric applications for the qualitative and quantitative investigation of grapevine organs. *Frontiers in Plant Science* 12. doi:10.3389/fpls.2021.723247.
- Varão Moura, A., A. Aparecido Rosini Silva, J. Domingos Santo da Silva, L. Aleixo Leal Pedroza, J. Bornhorst, M. Stiboller, T. Schwerdtle, and P. Gubert. 2022. Determination of ions in *Caenorhabditis elegans* by ion chromatography. *Journal of Chromatography B* 1204:123312. doi:10.1016/j.jchromb.2022.123312.
- Vasant Naik Bharati Vidyapeeth, V., M. K. Bayabai Shripatrao Kadam Kanya Mahavidyalaya, V. T. Aparadh Shri Pancham Khemaraj Mahavidyalaya, and B. A. Karadge. 2014. Methodology in determination of oxalic acid in plant tissue: A comparative approach. *Journal of Global Trends in Pharmaceutical Sciences Journal* 5 (2):1662–72. [Online]. <https://everythingcomputerscience.com/books/regmods/pdf>.
- Vermonti, N. 2022. *Structural and functional attributes of heuweltjies in the fynbos and succulent karoo biomes: The interaction of termites, vegetation and geochemistry*. Stellenbosch: Stellenbosch University.
- Verrecchia, E. P., O. Braissant, and G. Cailleau. 2006. The oxalate-carbonate pathway in soil carbon storage: The role of fungi and oxalotrophic bacteria. *Fungi in Biogeochemical Cycles* 9780521845 (January):289–310.
- Viscarra Rossel, R. A., D. J. J. Walvoort, A. B. McBratney, L. J. Janik, and J. O. Skjemstad. 2006. Visible, near infrared, mid infrared or combined diffuse reflectance spectroscopy for simultaneous assessment of various soil properties. *Geoderma* 131 (1–2):59–75. doi:10.1016/j.geoderma.2005.03.007.
- Vives-Peris, V., C. de Ollas, A. Gómez-Cadenas, and R. Pérez-Clemente. 2020. Root exudates: From plant to rhizosphere and beyond. *Plant cell reports* 39 (1):3–17. doi:10.1007/s00299-019-02447-5.
- Volmer, M., A. Bolck, B. G. Wolthers, A. J. de Ruiter, D. A. Doornbos, and W. van der Slik. 1993. Partial least-squares regression for routine analysis of urinary calculus composition with Fourier transform infrared analysis. *Clinical Chemistry* 39 (6):948–54. doi:10.1093/clinchem/39.6.948.
- Volmer, M., J. C. M. De Vries, and H. M. J. Goldschmidt. 2001. Infrared analysis of urinary calculi by a single reflection accessory and a neural network interpretation algorithm. *Clinical Chemistry* 47 (7):1287–96. doi:10.1093/clinchem/47.7.1287.